S. Afr. J. Chem., 2012, **65**, 39–49,
<http://journals.sabinet.co.za/sajchem/>.

The Synthesis of Nitrogen-Doped Multiwalled Carbon Nanotubes Using an Fe-Co/$CaCO_3$ Catalyst

Z.N. Tetana[a], S.D. Mhlanga[a], G. Bepete[a], R.W.M. Krause[b] and N.J. Coville[a,*]

[a]*DST/NRF Centre of Excellence in Strong Materials and the Molecular Sciences Institute, School of Chemistry, University of the Witwatersrand, Johannesburg, WITS, 2050, South Africa.*
[b]*DST/NRF Centre of Excellence in Strong Materials, Department of Chemical Technology, University of Johannesburg, P.O. Box 17011, Doornfontein, 2028, South Africa.*

Received 11 August 2011, revised 12 December 2011, accepted 30 January 2012.

Submitted by invitation to celebrate 2011 the 'International Year of Chemistry'.

ABSTRACT

A CVD method was used to prepare high-quality nitrogen-doped multiwalled carbon nanotubes (N-MWCNTs) using acetonitrile as the nitrogen and carbon source and acetylene as a carbon source over an Fe-Co/$CaCO_3$ catalyst in the temperature range 700–850 °C. This represents a continuation of earlier work in which Fe-Co on $CaCO_3$ was used to make undoped carbon nanotubes. The effect of synthesis parameters (growth temperature and CH_3CN vaporization temperature) on the yield, size, quality, morphology and thermal stability of the N-MWCNTs was studied. The resulting materials were characterized by TEM, SEM, TGA, BET, XPS, CN elemental analysis and Raman spectroscopy. TEM analysis revealed that the nanotubes exhibit bamboo-like structures with rough surfaces and a relatively uniform diameter. The bamboo compartment distance decreased with increase in synthesis temperature due to the increased nitrogen content in N-MWCNTs. The SEM examination showed that at high synthesis temperatures carbon spheres (CSs) with chain-like morphology and large sizes were also formed along with the N-MWCNTs. The XPS and CN elemental analysis revealed that nitrogen atoms were successfully doped into the carbon walls. The amount of nitrogen incorporated in the N-MWCNTs varied with increasing growth time and CH_3CN vaporization temperature.

KEYWORDS

Carbon nanotubes, CVD synthesis, nitrogen doping, acetonitrile, Fe-Co/$CaCO_3$ catalyst.

1. Introduction

Since the discovery of polyhedral carbon clusters (fullerenes) in 1985,[1] new graphite-like nanostructures such as carbon nanotubes (CNTs)[2] and related nanostructures (spheres,[3] onions,[4] fibres,[5] horns[6], etc.) have been reported. CNTs have attracted the attention of scientists in recent years for their application as catalyst supports,[7,8] nanoscale semiconductor devices,[5,9] sensors,[7,10,11] in hydrogen storage,[12,13] scanning probes,[14] etc. More importantly, while single-walled carbon nanotubes (SWCNTs) can either be metallic or semiconducting, depending on their chirality and diameter,[15,16] multiwalled carbon nanotubes (MWCNTs) present anisotropic metallic behaviour.[17] Doping of CNTs with heteroatoms provides a means of modifying the conducting and other properties of the CNTs.[18,19] Novel electronic properties can be expected if N atoms directly substitute C atoms in the graphitic lattice as the doping results in a production of an n-type conductor.[20] A high nitrogen content in CNTs leads to an increase in the CNT conductivity due to the rise of the Fermi level towards the conduction band.[21,22] Low dopant concentrations have been incorporated within the CNTs,[23] and the electronic conductance was shown to be significantly enhanced without altering the mechanical properties.[24] Nitrogen-containing CNTs have recently been reported by Gong and co-workers to be an efficient metal-free catalyst for the oxygen reduction reaction (ORR).[25] It has been reported that nitrogen-doped multiwalled CNTs (N-MWCNTs) are thermally less stable[26] and possess larger surface-active group/volume ratios, better mechanical properties, and better biocompatibility compared to undoped CNTs.[21,25,27]

Various synthesis methods have been used to make nitrogen-doped CNTs. These include arc discharge,[28] laser ablation,[29] substitution reactions,[30] catalytic pyrolysis of organic precursors including acetonitrile,[31] pyridine,[24] triazine,[32] and various chemical vapour deposition (CVD) methods.[33] The CVD method remains the most promising method for the commercial production of highly dense and well aligned nitrogen-doped CNTs by catalytic decomposition of suitable carbon and nitrogen sources. The growth process usually involves heating a catalyst (typically to 700–1000 °C) in an atmosphere of C and N containing precursors.

To date, N-doped MWCNTs have been synthesized by thermal CVD of a nitrogen-containing organic compound in the presence of supported metal nanoparticles, by the pyrolysis of acetonitrile over an Fe/MgO catalyst,[34] by using a Co-based catalyst derived from Co/Al layered double hydroxides using methane and acetonitrile as C and N sources, respectively,[35] by using a mixture of C_2H_6/Ar/NH_3 and an Fe/Al_2O_3 catalyst,[36] by using NH_3 and CH_4 over an Fe-Mo/MgO catalyst,[37] etc. Bamboo-like CNTs have recently been synthesized by thermal decomposition of pyridine and iron phthalocyanine over an iron catalyst under an ammonia atmosphere.[38] X-ray photoelectron spectroscopy (XPS) analysis of these N-CNT samples has demonstrated three types of nitrogen atoms associated with the CNT surface,

* To whom correspondence should be addressed. E-mail: neil.coville@wits.ac.za

namely pyridine-like, graphite-like, and molecular nitrogen; the maximum dopant concentration was found to be in the range of 1.18–3.22 at. % over the temperature range 750–875 °C.[38] Floating catalyst CVD methods have also been proven to be a popular method to make N-CNTs. For example, Nxumalo and co-workers prepared bamboo-shaped MWCNTs by the floating catalyst CVD method using ferrocene/aniline mixtures at 900 °C.[26]

In the CVD processes, when transition metal particles are used as a catalyst, it is believed that the CNT forms from the metal catalyst surface that resides at either the base[39] or the tip of a growing nanotube.[40] N-CNTs are proposed to grow only *via* a base growth process. Nitrogen-doping significantly alters the morphology of CNTs, typically leading to bamboo-like structures that contain regularly arranged compartments with a hollow channel.[19] It was proposed that the bamboo-like structures might be due to effects related to the catalyst particle shape, the bulk diffusion of carbon and nitrogen in the catalyst, or the slow movement of the catalyst compared to the growth rate of the CNT. It has been shown that the cup separation distance in the bamboo structure correlated with the concentration of the nitrogen in the tube.[26]

The nature of the support used during CNT synthesis plays an important role in influencing the activity of the catalyst. A number of factors need to be considered when choosing a support material, including thermal stability, solubility in acids/alcohol/water, surface area, etc.[41] High surface area materials such as SiO_2 and Al_2O_3 provide excellent supports for catalytic CNT production.[42] However, they are not easily removed and therefore purification of CNTs made from these supports remains a challenge.

Undoped MWCNTs have been produced by decomposing a hydrocarbon gas (e.g. acetylene) over a metal catalyst supported on $CaCO_3$ such as Ni/$CaCO_3$,[43] Co/$CaCO_3$,[43,44] Fe-Co/$CaCO_3$,[41,44] and Fe/$CaCO_3$.[44,45] At the end of the reaction the CaO can be easily dissolved in dilute acids such as HNO_3 and HCl. Further, studies revealed that Fe-Co catalysts are more effective than either Fe or Co catalysts when supported on $CaCO_3$.[46–49] The success in using $CaCO_3$ as a support suggested it could also be used to make N-MWCNTs.

In this study, we report on a systematic synthesis of N-MWCNTs by the thermal decomposition of acetylene (C_2H_2) and acetonitrile (CH_3CN) as the carbon and nitrogen sources over an Fe-Co/$CaCO_3$ catalyst, under an N_2 atmosphere. This study revealed the key roles played by CH_3CN concentration and reaction temperature on the structure and quality of the materials formed that permit a control of nitrogen content in the N-MWCNTs. This work represents a continuation of earlier work in which an Fe-Co on $CaCO_3$ was used to make undoped carbon nanotubes.[41]

2. Experimental

2.1 Catalyst Preparation

The Fe-Co/$CaCO_3$ catalyst was prepared by an impregnation route using an aqueous mixture of $Fe(NO_3)_3{\cdot}9H_2O$ and $Co(NO_3)_2{\cdot}6H_2O$.[41] The two metal nitrates (purchased from Sigma-Aldrich) were of analytical reagent grade and were used without further treatment. Calculated amounts of the metal nitrates were mixed and dissolved in distilled water to make a 0.3 M Fe-Co (50:50 w/w) precursor solution. This precursor solution was added dropwise to the stirred $CaCO_3$ and the mixture was left to stir for 30 minutes. The resulting metal-support mixture was then filtered and dried in an oven at 120 °C for 12 hours, cooled to room temperature, ground and sieved using a 150 μm mesh sieve. The catalyst was then calcined at 400 °C for 16 hours in air to decompose the nitrates in the catalyst. The total loading of the Fe-Co catalyst on the $CaCO_3$ was 5 mass %. These catalysts were completely characterized as reported in our earlier paper.[41]

2.2 Fabrication and Purification of N-MWCNTs

N-MWCNTs were synthesized using a procedure similar to that reported by Mhlanga *et al.* for the synthesis of undoped MWCNTs.[41] The syntheses were carried out in a tubular quartz reactor (51 cm × 1.9 cm i.d.) placed in a horizontal furnace. C_2H_2 (Afrox) and CH_3CN (Sigma-Aldrich) were used as carbon and carbon/nitrogen sources, respectively. N_2 (Afrox) was used as a carrier gas to dilute the C_2H_2 in order to decrease the contact time between C_2H_2 and the catalyst, and consequently reduce the formation of amorphous carbon.[50] For each synthesis, 0.3 g of the catalyst was uniformly spread onto a quartz boat (120 mm × 15 mm) which was then placed in the centre of the quartz tube. A series of experiments were performed, using different acetonitrile vaporization temperatures (room temperature, 50 °C and 80 °C) and different reaction temperatures (700, 750, 800 and 850 °C). The furnace was raised to a desired temperature at 10 °C min^{-1} under flowing N_2 gas (40 mL min^{-1}) in the reaction. Once the desired temperature was reached, the N_2 (240 mL min^{-1}) and C_2H_2 (100 mL min^{-1}) were simultaneously bubbled through CH_3CN for 1 hour. After this, the bubbling of the gases through CH_3CN was stopped and the system was left to cool down to room temperature under N_2 (40 mL min^{-1}). The quartz boat was then removed from the reactor and the carbon deposits that formed along with the catalyst were weighed. Other forms of carbon materials were made when the reaction and acetonitrile heating temperatures were set to 900 °C and 80 °C, respectively. The resulting nitrogen-containing materials were purified using 55 % HNO_3 under reflux in an oil bath held at 110 °C for 4 hours to remove the CaO, residual Fe-Co particles and introduce oxygen surface groups. The acid-treated carbon materials were then filtered and washed several times with distilled water (to remove the residual HNO_3) until the pH of the filtrate was neutral. The nitrogen-containing materials were dried at 120 °C for 12 hours. As-synthesized N-MWCNTs grown at 700–850 °C using CH_3CN are denoted as 700, 750, 800 and 850, and the purified materials are denoted as 700P, 750P, 800P and 850P.

2.3 Carbon Yield Calculation

The yield was determined by estimating the amount of carbon reactants used and the amount of carbon produced. The carbon was contained in both reactants (C_2H_2, CH_3CN). The yield was determined from the unpurified reactants produced. The yield calculated includes carbon formed as both CNTs and carbon spheres (CSs), (see online supplement for calculations).

2.4. Characterization of N-MWCNTs

The morphology and structural features of the nitrogen-containing nanotubes were ascertained by transmission electron microscopy (TEM) using a FEI Technai G^2 Spirit electron microscope operated at 120 kV, scanning electron microscopy (SEM) using a FEI QUANTA 400 FEG ESEM at 5 kV, and Raman spectroscopy using a Jobin-Yvon T6400 micro-Raman spectrometer equipped with a liquid nitrogen cooled charge coupled device detector. The thermal stability of the N-MWCNTs was investigated by thermogravimetric analysis (TGA) using a Perkin Elmer Pyris 1 TGA. About 10 mg of each sample was heated to 900 °C at a rate of 10 °C min^{-1} under air. The mass of all samples was kept

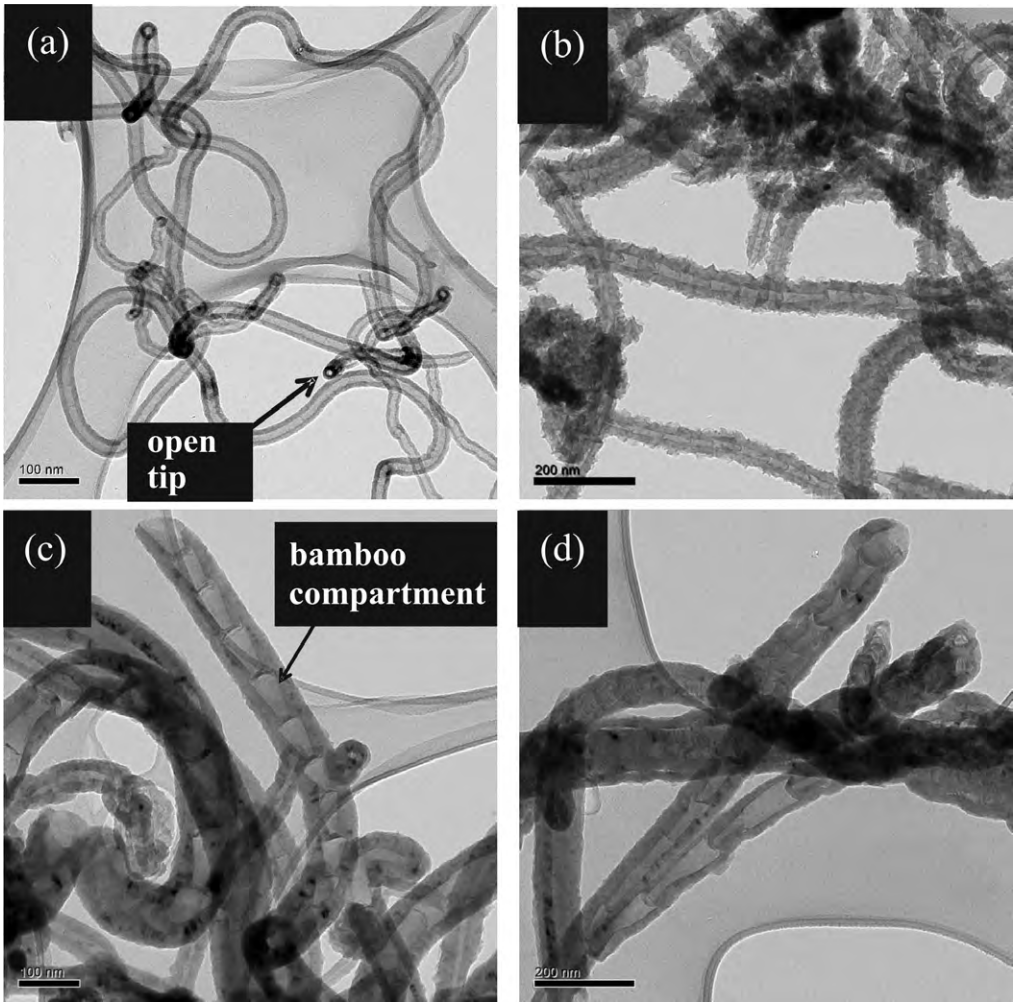

Figure 1 TEM images of the purified N-MWCNTs grown using CH_3CN (r.t.) and reaction temperatures of (**a**) 700 °C, (**b**) 750 °C, (**c**) 800 °C and (**d**) 850 °C.

constant (*ca.* 10 mg) in order to reduce the effects of variability in measurements. BET surface areas of the N-MWCNTs (~200 mg for each measurement) were obtained through N_2 adsorption using an ASAP 2000 Micrometrics TriStar Surface Area and Porosity Analyzer. The nitrogen concentration was determined by CN elemental analysis using a Carlo Erba NA 1500 Nitrogen Carbon Sulphur Analyzer at the ARC– Institute for Soil, Climate and Water in Pretoria. The X-ray photoelectron spectroscopy (XPS) measurements were performed in a Thermo Scientific K-Alpha equipped with a monochromatic Al Kα X-ray source (1486 eV photons and 200 μm spot size), at the Department of Physics and Astronomy, Rutgers University, USA.

3. Results and Discussion

3.1. Structural Analysis of N-MWCNTs

Figures 1–3 show TEM images of the nitrogen-containing CNTs prepared from acetonitrile at different temperatures. It was observed that the quality of the N-MWCNTs varied as the reaction temperature increased. All the N-MWCNTs synthesized at 700–750 °C were light and spongy in texture, while all the materials prepared at 800–850 °C were coarser in texture. As mentioned in the experimental section, the as-synthesized N-MWCNTs were purified with HNO_3 to remove the CaO and residual Fe-Co particles. After purification, no significant changes to the structures and the sizes of the N-MWCNTs were observed. TEM analysis revealed that at all temperatures, the CNTs were multiwalled, randomly arranged and were found to have open ends. These open-ended N-MWCNTs may be suitable for field emission studies.[51] All the unpurified nanotubes formed contained no residual catalyst particles in their tips, suggesting that they were made *via* a base-growth mode involving a strong interaction between Co-Fe particles and the CaO.[41,52]

Nitrogen incorporation is evidenced by the presence of bamboo-like structures in which the inside of the tube is separated into a series of compartments (Figs 1–3). Doping leads to the introduction of defects and a higher degree of disorder in the graphite tubes.[26] Evaluation of the TEM image compartment size indicates that the degree of doping increased at higher reaction and CH_3CN temperatures. However, the observed increase in nitrogen incorporation with increase in growth temperatures above 750 °C contradicts other findings in the literature. The findings in the literature suggest that as the growth temperature increases, the nitrogen content decreases.[53,54] The contradiction can be related to the difference in synthesis methods, catalysts, experimental parameters, and C and N precursors used in this study. The images also reveal that with the increase of temperature from 700–750 °C (Figs 1a, 1b, 2a, 2b, 3a and 3b) roughening of the outer N-MWCNTs surfaces is more prominent but roughening decreases as temperature increases from 800–850 °C (Figs 1c, 1d, 2c, 2d, 3c and 3d).

At 700 °C the tubes appear to have thin walls and very few compartments. The percentage of nitrogen in these tubes is ~2.2 % (see later). The N-MWCNTs grown at 750 °C at all CH_3CN

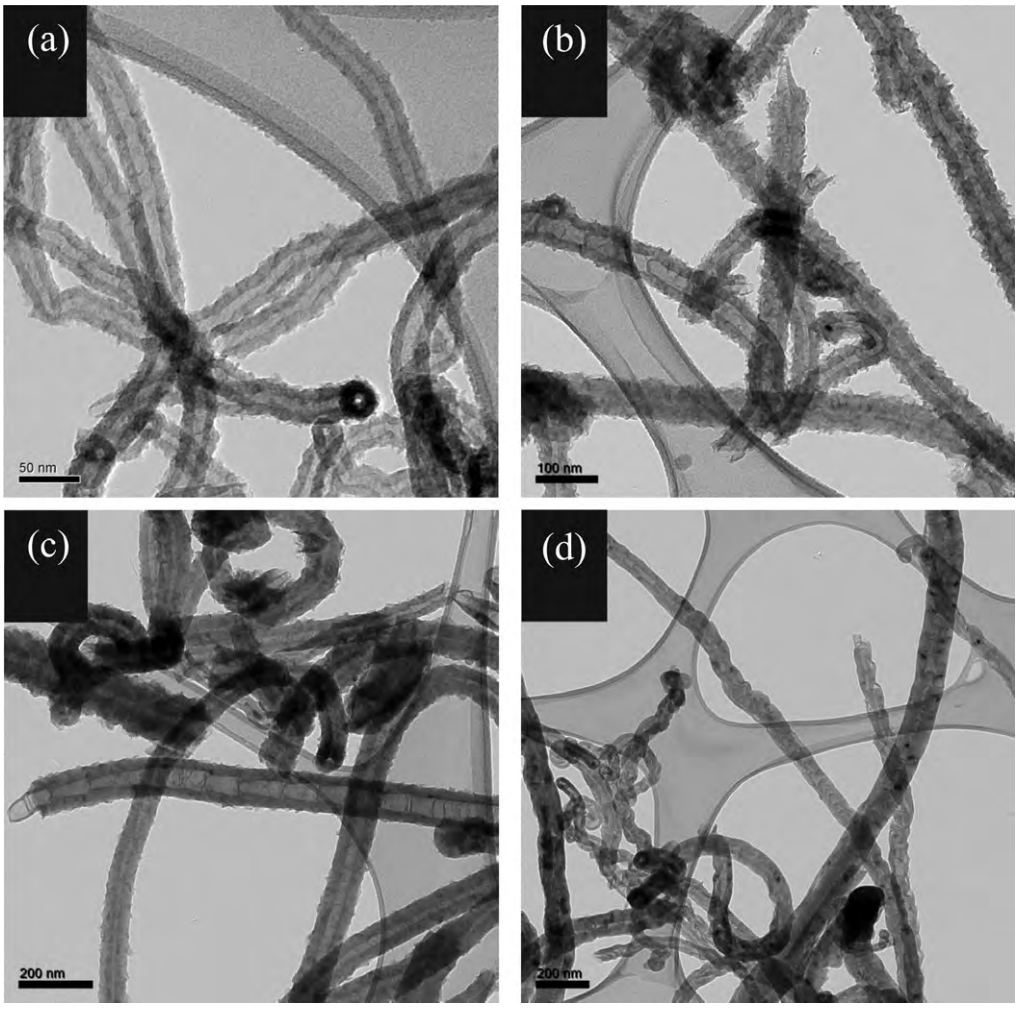

Figure 2 TEM images of the purified N-MWCNTs grown using CH_3CN (50 °C) and reaction temperatures of (**a**) 700 °C, (**b**) 750 °C, (**c**) 800 °C and (**d**) 850 °C.

heating temperatures (room temperature to 80 °C; Figs 1b, 2b and 3b), have very rough surfaces and gave compartments that were separated by narrow shells, formed randomly and frequently. At 800 °C (Figs 1c, 2c and 3c), as the CH_3CN vaporization temperature increased from room temperature to 80 °C, the compartment layers occurred at regular distances and became more visible and appeared to be thick and curved. At 850 °C, as the CH_3CN heating temperature increased from room temperature to 80 °C, the well-curved, thick compartment layers had shorter separation distances (Figs 1d, 2d and 3d). The N-MWCNTs at 850 °C had a wide range of outer diameters that decreases with CH_3CN heating temperature. At 850 °C carbon spheres (CSs) were observed, also with a wide range of diameters (see Table 1).

Quantification of the above TEM observation was achieved by analysis of the nitrogen-containing carbon nanotubes from the TEM images (supplementary Figures S1a–c and Table 1). The data reveal that at all CH_3CN heating temperatures, as the synthesis temperature increased, the outer diameters of the N-MWCNTs also increased. On the other hand, the inner diameter measurements revealed no systematic trend with respect to synthesis and CH_3CN temperatures. It is noted that at all CH_3CN temperatures, the average outer diameters of the N-MWCNTs synthesized at 700, 750, 800 and 850 °C, are relatively uniform in size (±5 nm of the average value).

Figure 4 and supplementary Fig. S2 show representative SEM micrographs of the purified nitrogen-containing materials synthesized at 850 °C (using CH_3CN at r.t. and 50 °C) and 800–850 °C (using CH_3CN at 80 °C), respectively. The SEM images show that CSs were formed along with N-MWCNTs. The CSs were linked together in a necklace-like fashion, typical of CSs synthesized in the presence of hydrocarbons by CVD; in the absence of a catalyst.[55]

Quantitative observation of TEM and SEM images of carbon produced at 850 °C indicates that the N-MWCNT/CS ratio varied with CH_3CN heating temperature. At room temperature the N-MWCNT/CS ratio was 70/30, at 50 °C it was 65/35 and at 80 °C it was 50/50. (At a reaction temperature of 800 °C, using CH_3CN at 80 °C, the ratio was 60/40). The SEM images and Table 1 show that (i) increasing CH_3CN vaporization temperature gives CSs with a larger yield and diameters, (ii) increasing growth temperature gives CSs with a larger yield and larger diameters. This is consistent with previous reports that higher temperatures favour growth of carbon spheres.[56,57] In independent studies, nitrogen-doped carbon spheres (N-CSs) have been synthesized in our laboratory using C_2H_2 and CH_3CN without the use of a catalyst. This confirms that the CSs formed here have been produced *via* non-catalytic synthesis procedures and contain nitrogen.

3.2. Yield of N-MWCNTs

In this study the yields have been determined from the amount of carbon deposited relative to the amount of carbon passed over the catalyts, e.g. a yield of 16 % was obtained at

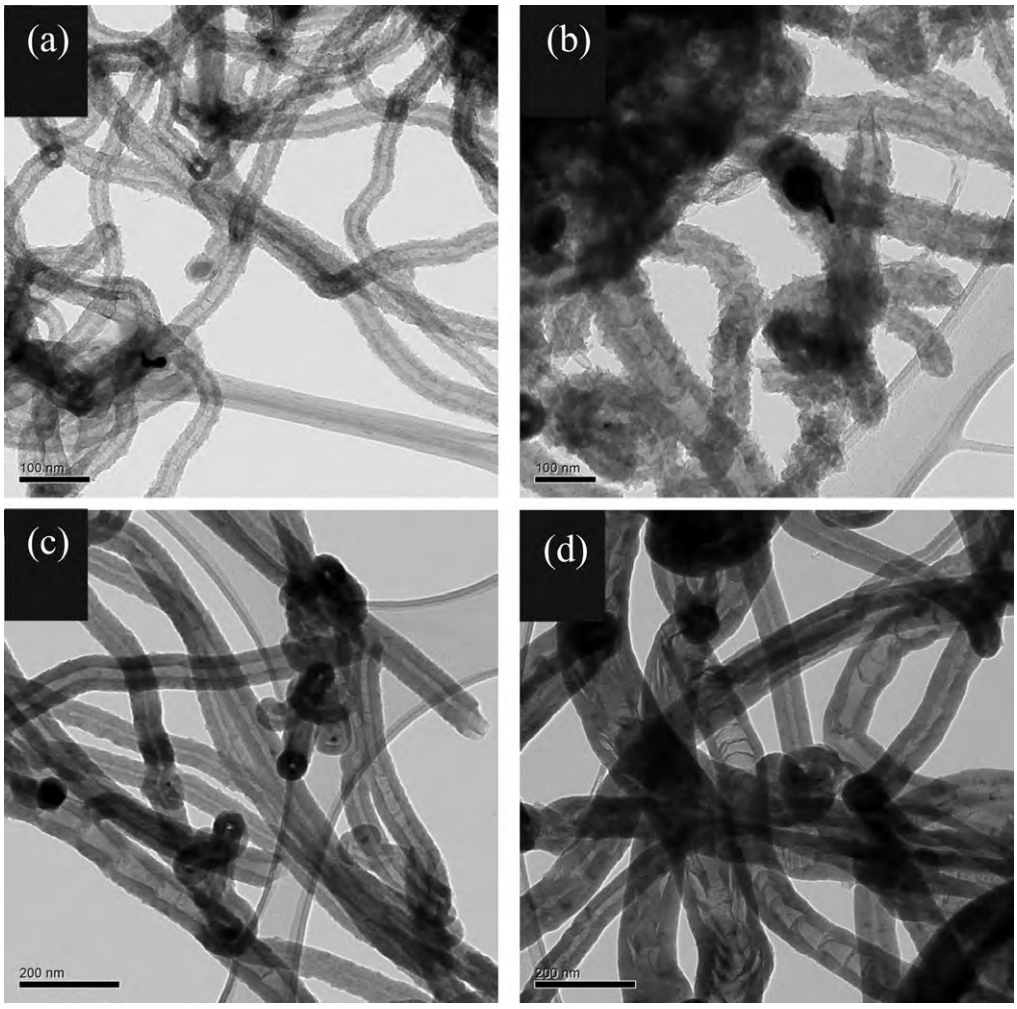

Figure 3 TEM images of the purified N-MWCNTs grown using CH_3CN (80 °C) and reaction temperatures of (**a**) 700 °C, (**b**) 750 °C, (**c**) 800 °C and (**d**) 850 °C.

800 °C. The yields are typical of N-CNT yields found in these types of reactions. Yields are often quoted as the amount of product formed relative to the amount of catalyst used (a type of turn over number) and then the 'yield' can be >1000 %.[58]

In catalytic CVD procedures, higher temperatures are used to produce a higher carbon yield.[55] However, at higher temperatures non-catalytic competing pathways can occur and in this study CSs formed together with the desired materials. The total yield of the as-synthesized nitrogen-containing materials increased as the synthesis temperature increased from 700–850 °C (Fig. 5). At low reaction temperatures (700–750 °C), only small amounts of N-MWCNTs were formed. At higher temperatures (800–850 °C), the decomposition rate of C_2H_2 and CH_3CN is faster and large amounts of N-MWCNTs and N-CSs were formed. An increased CH_3CN content is seen to reduce the carbon yield (Fig. 5).

3.3. BET Surface Area and Pore Volume Analysis of N-MWCNTs

The specific surface areas and pore volume of the purified N-MWCNTs are shown in Table 2. The surface areas and pore volume of the purified N-MWCNTs decreased as (i) reaction temperature and (ii) CH_3CN temperature increased from 700–850 °C and r.t. to 80 °C, respectively. The observed surface

Table 1 Effects of temperature on the outer diameter of purified N-MWCNTs.

	CH_3CN temperature								
	r.t.			50 °C			80 °C		
Sample	Size distribution /nm	Average diam. /nm	Type of material	Size distribution /nm	Average diam. /nm	Type of material	Size distribution /nm	Average diam. /nm	Type of material
700	22–98	30	CNTs	22–118	30	CNTs	22–158	30	CNTs
750	22–98	50	CNTs	22–138	50	CNTs	22–178	50	CNTs
800	17–143	70	CNTs	22–158	70	CNTs	40–170	70	CNTs
							75–350	100	CSs
850	22–220	90	CNTs	5–195	90	CNTs	42–220	90	CNTs
	100–450	150	CSs	80–450	130	CSs	200–450	250	CSs

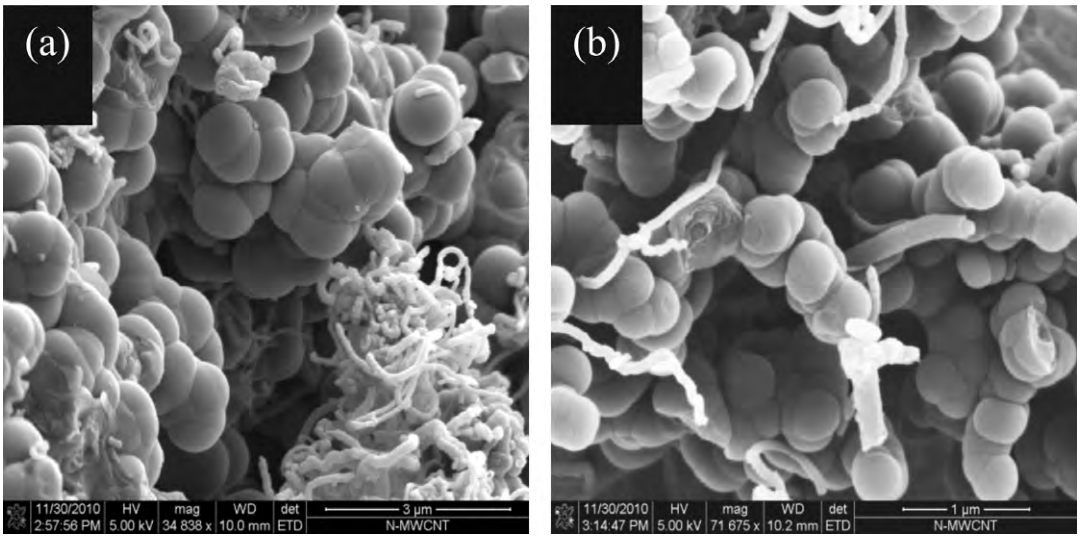

Figure 4 SEM images of the purified N-MWCNTs grown at 850 °C using CH_3CN at (**a**) r.t. and (**b**) 50 °C.

areas and pore volume of the N-MWCNTs are related to (i) the formation of oxidized functional groups on the surface of N-MWCNTs,[59,60] (ii) the larger average diameters of the N-MWCNTs, which exhibit a lower external surface area at higher synthesis temperatures, (iii) the harder texture and (iv) the presence of low surface area N-CSs.

3.4. Thermogravimetric Analysis of N-MWCNTs

The thermal stabilities of the as-synthesized and purified N-MWCNTs were evaluated using TGA under an air flow rate of 30 mL min^{-1} and a constant heating rate of 10 °C min^{-1}. TGA was also used to study the overall purity of the N-MWCNTs. Figures 6a–c show typical TGA profiles and the corresponding derivative curves of the as-synthesized N-MWCNTs made at 700–850 °C using CH_3CN at r.t., 50 °C and 80 °C. The TGA profiles of the purified N-MWCNTs (denoted 700P–850P) are shown in supplementary Figs S3–S5. The maxima in the first order derivative plots of the TGA curves were used to estimate decomposition temperatures of the N-MWCNTs (Table 3).[61]

According to the literature, amorphous carbon typically oxidizes in air at temperatures below 400 °C,[62,63] whereas CNTs oxidize at higher temperatures, up to 800 °C.[64] The TGA data showed that there was no mass loss below 400 °C, confirming (from TEM studies) that amorphous carbon was not observed in the as-synthesized N-MWCNTs. All N-MWCNTs synthesized at 700 °C (Figs 6a–c) showed weight gains at 455–553 °C due to the formation of metal oxide from incompletely oxidized catalysts.[65]

Two weight loss derivative curves occur in the high temperature region for all the as-synthesized N-MWCNTs and the peak positions vary with temperature. As seen from Table 3, the first peak of the derivative plot occurs at 587–700 °C for all the as-synthesized N-MWCNTs and can be attributed to the degradation of N-MWCNTs while the second peak at 737–768 °C can be attributed to other carbon crystalline materials such as graphitic soot,[66] and possibly undoped MWCNTs.

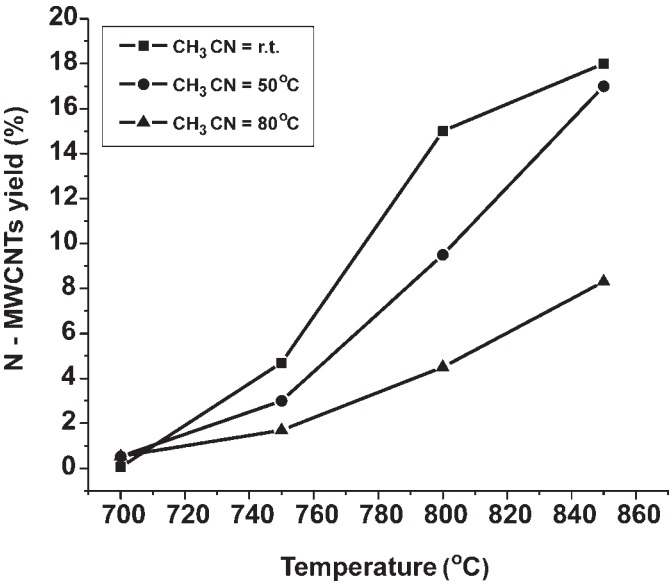

Figure 5 Graph showing the amounts of N-MWCNTs grown at 700–850 °C using CH_3CN at r.t., 50 °C and 80 °C.

For all purified N-MWCNTs synthesized using CH_3CN at r.t. and 50 °C, the carbon decomposition temperature generally increased as the reaction temperature increased from 700–800 °C and decreased at 850 °C. Moreover, when the CH_3CN heating

Table 2 BET surface areas and pore volume of the purified N-MWCNTs.

	CH_3CN temperature					
	r.t.		50 °C		80 °C	
Sample	BET surface area /m^2 g^{-1}	Pore volume /cm^3 g^{-1}	BET surface area /m^2 g^{-1}	Pore volume /cm^3 g^{-1}	BET surface area /m^2 g^{-1}	Pore volume /cm^3 g^{-1}
700P	138.4	0.55	142.6	0.48	97.3	0.32
750P	64.8	0.24	60.6	0.16	56.3	0.26
800P	29.6	0.076	18.1	0.060	16.5	0.056
850P	10.9	0.039	16.3	0.042	9.2	0.026

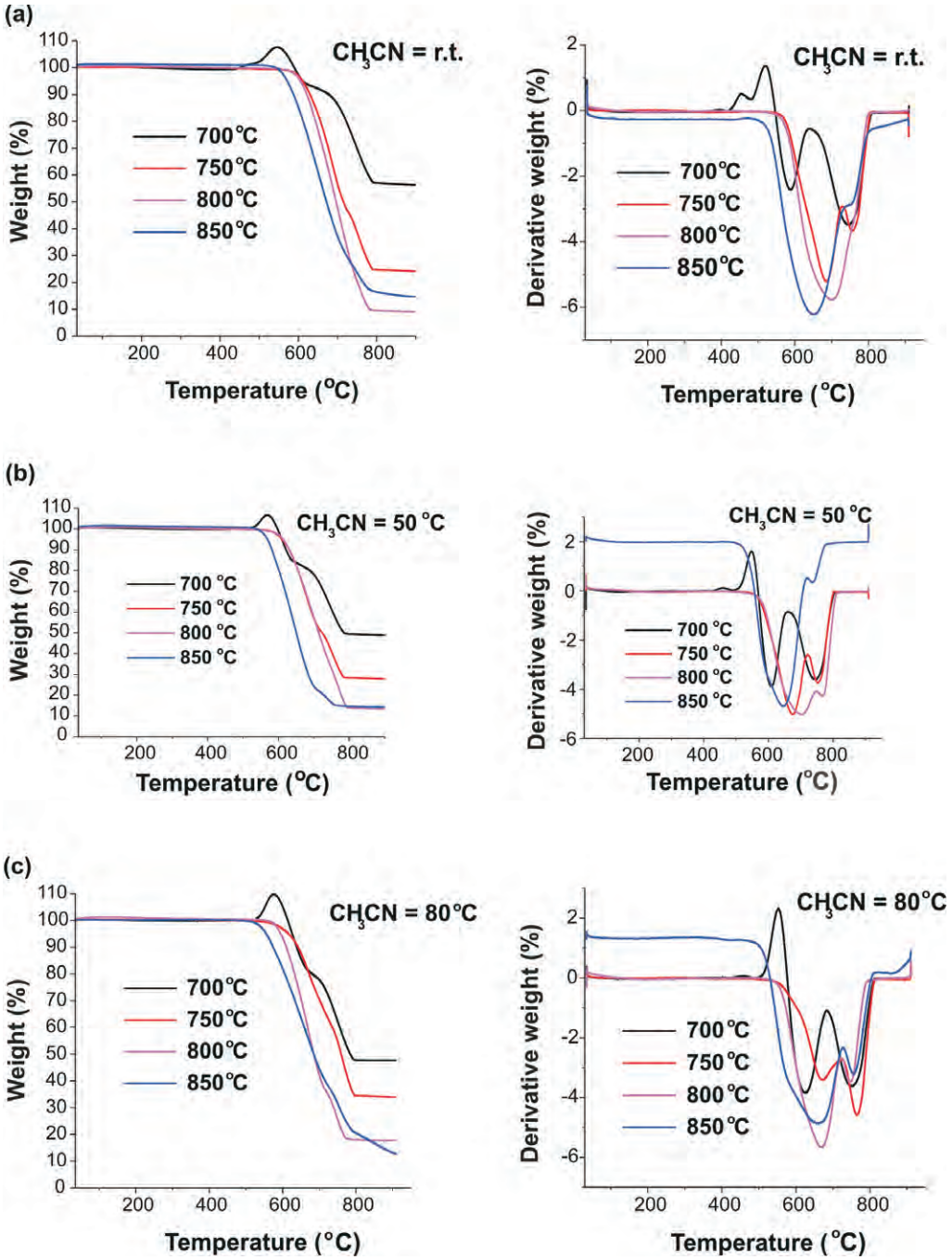

Figure 6 TGA and corresponding derivative profiles of the as-synthesized N-MWCNTs using CH_3CN at (**a**) r.t., (**b**) 50 °C and (**c**) 80 °C.

temperature was kept at 80 °C, the decomposition temperature was more variable. Our TGA results generally agree with those reported in the literature. A number of reports suggested that an increase in nitrogen content gave rise to less thermally stable N-CNTs, due to more structural defects and disorder achieved by the introduction of reactive sites in the N-CNTs.[67,68]

The general drop in decomposition temperature at 850 °C is associated with the presence of a mixture of N-MWCNTs and CSs in the products (see Table 3). Usually small diameter CNTs or small bundles of the CNTs have lower combustion temperatures.[69] It is evident from our results that lower diameter N-MWCNTs, formed at a low growth temperature, decompose at a lower temperature than the large diameter N-MWCNTs prepared at a high growth temperature.[70] The results in Table 3 indicate a significant effect of CH_3CN vaporization temperature on the decomposition temperature of the as-synthesized N-MWCNTs. As can be seen, the as-synthesized N-MWCNTs at 700 °C show ~50 % impurities (mainly Fe-Co/$CaCO_3$) but the yield of the impurities decreased as the synthesis temperature increased to 850 °C (~6 % impurities). A large amount of the residual metal catalyst particles (Fe_2O_3 and Co_3O_4) was observed at lower synthesis temperatures at all CH_3CN heating temperatures.

The weight loss derivative curves of the purified N-MWCNTs (supplementary Figs S3–S5) showed no weight gains due to metal oxide formation, indicating that HNO_3 was effective in removing Co and Fe from the N-MWCNTs. It was also observed that after acid-treatment of all N-MWCNTs, the amount of residual catalyst decreased as the synthesis temperature increased, suggesting that the residual Fe_2O_3 and Co_3O_4 catalyst particles were mostly removed. As shown in Table 3 and supplementary Figs S3–S5, the acid-treated N-MWCNTs oxidized earlier than

Table 3 Decomposition temperatures and residual masses (determined by TGA) of the as-synthesized and purified N-MWCNTs.

	CH_3CN temperature					
	r.t.		50 °C		80 °C	
Sample	Decomposition temperature /°C	Residual mass /%	Decomposition temperature /°C	Residual mass /%	Decomposition temperature /°C	Residual mass /%
700	587	56	611	49	623	48
700P	582	3.1	591	1.4	601	5.9
750	684	24	674	28	671	34
750P	662	0.38	626	3.4	636	2.0
800	697	8.9	703	13	668	18
800P	633	0	687	5.2	598	9.0
850	652	6.0	645	5.6	660	12
850P	626	0.38	668	2.0	658	1.5

Table 4 CN elemental analysis of the purified N-MWCNTs.

	CH_3CN temperature					
	r.t. Atomic %		50 °C Atomic %		80 °C Atomic %	
Sample	C	N	C	N	C	N
700P	78.24	2.23	86.58	2.16	84.78	2.14
750P	88.89	1.44	86.91	1.76	89.82	1.68
800P	91.11	1.98	87.85	2.22	82.90	2.81
850P	88.39	3.46	94.55	3.64	87.18	4.18

the as-synthesized N-MWCNTs. This can be attributed to the presence of –OH and –COOH functional groups on the tubes, which assist the decomposition of the CNTs.

3.5. Elemental (C and N) Analysis of N-MWCNTs

The purified nitrogen-containing carbon nanomaterials were also characterized by C and N elemental analysis. CN analysis confirmed the presence of nitrogen in the N-MWCNTs (Table 4). It is clear from the data that as the synthesis temperature increased (700 to 800 °C), the percentage of N inserted into the N-MWCNTs decreased and then increased. This arises from two effects: as the temperature increases the N doping of the CNTs decreases.[49,53]

However, at the higher temperatures, CSs form that also contain nitrogen. In independent studies,[71] it was shown that the N content of CSs increased slightly with increasing temperature. Thus, the two effects operate in opposite directions to give the results seen.

The data also showed that at 700 °C and 750 °C, as CH_3CN vaporization temperature increased (r.t. to 80 °C) the N concentration showed little variation, suggesting that the C_2H_2/CH_3CN ratio had little effect on the N-MWCNT growth.

3.6. Raman Spectroscopy Analysis of N-MWCNTs

Raman spectroscopy is an effective tool to analyse the crystallinity and the defects in carbon structures.[72] Raman spectroscopy was used to provide information on the degree of structural defects in N-MWCNTs (supplementary Figs S6–S8). The Raman spectra (also, see Table 5) show two main bands at approximately 1350–1360 cm^{-1} (D-band) and approximately 1590–1600 cm^{-1} (G-band), which are characteristic of MWCNTs. The D-band is associated with defects and impurities in the CNTs. The G-band corresponds to the stretching mode of the C-C bond in the graphite plane. The area ratio of the D- to G-bands (I_D/I_G) allows for a comparison of defects in the N-MWCNTs. A high I_D/I_G ratio indicates more defects present inside the carbon layers of CNTs. The results indicate that as the reaction temperature increases the degree of disorder increases, correlating with the higher nitrogen content (Table 4).

Table 5 D-, G-bands and I_D/I_G ratios of the as-synthesized and purified N-MWCNTs.

	CH_3CN temperature								
	r.t.			50 °C			80 °C		
Sample	D-band/cm^{-1}	G-band/cm^{-1}	I_D/I_G ratio	D-band/cm^{-1}	G-band/cm^{-1}	I_D/I_G ratio	D-band/cm^{-1}	G-band/cm^{-1}	I_D/I_G ratio
700	1352	1598	1.43	1352	1601	1.31	1354	1600	1.05
700P	1355	1595	1.44	1353	1595	1.48	1355	1597	1.52
750	1355	1600	1.41	1354	1597	1.48	1357	1601	1.47
750P	1354	1595	1.52	1352	1593	1.65	1363	1602	1.52
800	1361	1600	2.20	1360	1598	1.75	1361	1597	2.53
800P	1362	1599	1.72	1361	1594	1.87	1368	1604	1.92
850	1359	1592	2.15	1351	1614	1.68	1358	1591	1.55
850P	1359	1596	2.14	1355	1614	2.02	1360	1596	2.04

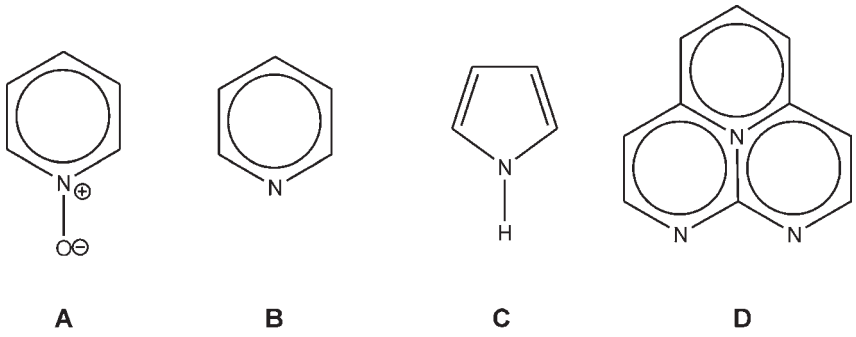

Figure 7 Types of nitrogen-based species that can be incorporated into graphitic carbon: (**A**) oxidized pyridinic, (**B**) pyridinic, (**C**) pyrrolic, (**D**) quaternary.[73]

3.7. XPS Analysis of Purified N-MWCNTs Grown at 800 °C Using CH_3CN at r.t.

XPS was used to determine the nitrogen-doping level and the types of N-moieties in the N-MWCNTs grown at 800 °C using CH_3CN at r.t. According to van Dommele and co-workers,[73] nitrogen can be incorporated into the CNT lattice in different bonding configurations (Fig. 7); namely, (A) pyridinic oxides: which are attributed to oxidized nitrogen on the graphite layers, (B) pyridine-like N: where the N atom is sp^2 hybridized, bonding to two C atoms, (C) pyrrole-like N: where the N is sp^3 hybridized in a five-membered ring, and (D) quaternary/graphitic/substitutional N: where a graphitic carbon atom is substituted by a N atom in the graphitic sheet.

XPS spectra of the purified N-MWCNTs grown at 800 °C using CH_3CN at r.t. are displayed in supplementary Fig. S9 and the results of the peak analysis are summarized in Table 6. Figure 8 shows the high-resolution N 1s XPS spectrum, which indicates the presence of nitrogen-based species on the N-MWCNTs. The N 1s peak can be deconvoluted into three peaks, representing molecular nitrogen intercalated within the walls or within the inner cavity of the CNTs (molecular N_2 at 405 eV)[74], quaternary nitrogen (N_Q at 401 eV) and pyridinic nitrogen (N_P at 398 eV).[75] The analysis of the N 1s spectra reveals that N atoms in the outer layer mainly exist as molecular N_2 (0.76 %). The N 1s peak also showed quaternary N (0.35 %) with a small portion of pyridinic N (0.21 %). This result is in line with other observations reported in the literature.[73,74,76] For example, van Dommele and co-workers,[73] when using CH_3CN and pyridine as N sources over Fe, Co or Ni supported on Al_2O_3 or SiO_2, established that quaternary nitrogen was found when nitrogen-doped CNTs were grown at high temperatures (750 and 850 °C), while pyridinic nitrogen was predominantly present at a lower temperature (550 °C). In addition, Yadav and co-workers[53] also established the presence of quaternary N when they synthesized bamboo-shaped CNTs using spray pyrolysis of ferrocene/acetonitrile solution at 850–950 °C. The total concentration of N from XPS analysis was 1.32 % (Table 6), consistent with the results of our CN elemental analysis (1.98 %, Table 4). Generally, an XPS spectrum mainly reflects the information of the outer layer of the measured sample. The combination of XPS and CN analysis results here suggests that nitrogen atoms appear uniformly doped from the interior to the surface of the N-MWCNT structure.

Table 6 XPS analysis of purified N-MWCNTs grown at 800 °C using CH_3CN at r.t.

Binding energy (eV) (and atomic concentration (%))		
C	N	O
284.70 (71.01 %)	398.68 (0.21 %)	531.81 (5.67 %)
288.56 (4.64 %)	401.45 (0.35 %)	533.61 (2.5 %)
287.19 (2.26 %)	404.98 (0.76 %)	532.91 (2.76 %)
286.12 (9.84 %)		

Carbon and oxygen were also identified by XPS analysis (Table 6, peaks at about 285–289 eV and 531–533 eV, respectively).

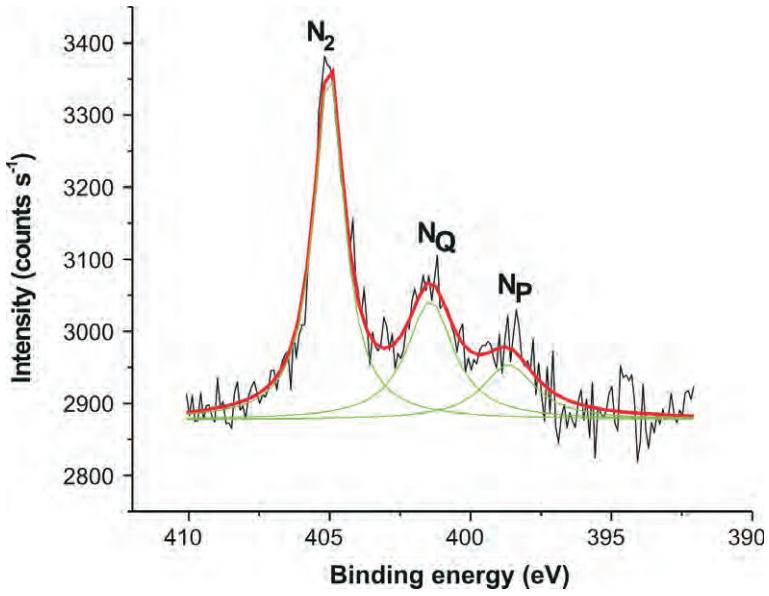

Figure 8 Deconvoluted N 1s XPS spectra of the purified N-MWCNTs synthesized at 800 °C using CH_3CN at r.t.

The strong C 1s peak at 284.7 eV can be assigned to sp^2 hybridized carbon (C-C bond) which is the major component in the N-MWCNTs. This value is similar to the previously reported for the N-CNTs by Ayala and co-workers.[75] The peaks at about 287 and 289 eV can be assigned to C-N bonding species[75] and O=C-O bond, respectively, due to the functionalization of N-MWCNTs by HNO_3. The O 1s peak at about 532 eV can be assigned to C-O and O-H bonds, also due to functionalization of N-MWCNTs by HNO_3. The oxygen peak is associated with C-O functionalities due to the oxygen absorbed on the surface of the CNTs,[77] the substrate on which the nanotubes were grown[78] and exposure of the sample to atmospheric air.[79]

4. Conclusions

Our results describe a simple method to make good yields of nitrogen-containing multiwalled carbon nanotubes with known nitrogen content. We have successfully synthesized nitrogen-doped carbon nanotubes by the catalytic pyrolysis of acetonitrile over a $CaCO_3$ supported Fe-Co catalyst. The CNTs formed were mostly multiwalled and bamboo-shaped. At higher temperatures (800–850 °C) a mixture of N-MWCNTs and CSs was observed. It is obvious that an increase in CH_3CN vaporization temperature plays a role in the formation of the nitrogen-containing materials. The study shows that the best conditions for the synthesis of high-quality N-MWCNTs in good yields are 800 °C and a r.t. CH_3CN vaporization temperature, as the conditions give pure N-MWCNTs in good yield. The presence of nitrogen in all N-MWCNTs was confirmed by CN elemental analysis. The results showed that N-doping increased with an increase in CH_3CN vaporization temperature.

XPS results revealed that the nitrogen atoms were successfully doped inside the carbon walls and are trigonally bonded to graphitic carbon atoms. CN analysis and XPS data suggested that nitrogen atoms were uniformly doped throughout the N-MWCNT structure. At high synthesis temperatures, nitrogen incorporation into carbon is higher than for samples synthesized at low temperatures. This can be related to the higher number of defects in their structure, as confirmed by Raman spectroscopy. It has been shown that the properties of N-MWCNTs, i.e. the level and the type of nitrogen-doping, surface area, diameter, quality and thermal stability, can be tuned by changing the growth and CH_3CN temperatures. The high surface area and thermal stability properties of the N-MWCNTs provide advantages for the N-MWCNTs to be used in several applications in catalysis. The N-MWCNTs synthesized are suitable for use as catalyst supports for the synthesis of chemicals, in water purification, as well as in fuel cell and solar cell applications. The method used here is environmentally friendly and suitable for large scale production of N-MWCNTs.

This work has shown that N-doped MWCNTs can be synthesized over an Fe-Co/$CaCO_3$ catalyst, suggesting that this method could be used to make other doped CNTs. The study shows that operating conditions need to be clearly established. Nitrogen-doping of the CNTs are limited to ~2 % using this procedure.

Acknowledgements

The authors would like to thank the National Research Foundation, DST/NRF Centre of Excellence in Strong Materials, CSIR and the University of the Witwatersrand for financial support. We gratefully acknowledge the Department of Physics and Astronomy at Rutgers University, USA, for XPS assistance and M.F. Philpott from the ARC– Institute for Soil, Climate and Water, for C and N elemental analysis. We also thank R.M. Erasmus for his assistance with Raman spectroscopy analysis. The technical support given by the University of the Witwatersrand Microscopy and Microanalysis Unit is also appreciated (special thanks are due to M.J. Witcomb, A. Ziegler and the late A.R. Seema).

References

1 H.W. Kroto, J.R. Heath, S.C. O' Brien, R.F. Curl and R.E. Smalley, *Nature,* 1985, **318**, 162–163.
2 S. Iijima, *Nature,* 1991, **354**, 56–58.
3 (a) D. Ugarte, *Nature,* 1992, **359**, 707–709; (b) Z.C. Kang and Z.L. Wang, *Philos. Mag. B,* 1996, **73**, 905–929; (c) Z.L. Wang and Z.C. Kang, *J. Phys. Chem.,* 1996, **100**, 17725–17731.
4 (a) N. Sano, H. Wang, M. Chhowalla, I. Alexandrou and G.A.J. Amaratunga, *Nature,* 2001, **414**, 506–507; (b) X.H. Chen, F.M. Deng, J.X. Wang, H.S. Yang, G.T. Wu and X.B. Zhang, *Chem. Phys. Lett.,* 2001, **336**, 201–204; (c) X. Bing-she, *New Carbon Mater.,* 2008, **23**, 289–301.
5 (a) A. Shaikjee, P.J. Franklyn and N.J. Coville, *Carbon,* 2011, **49**, 2950–2959; (b) A. Shaikjee and N.J. Coville, *Small,* 2011, **49**, 2950–2959; A. Shaikjee and N.J. Coville, 2012, *Mater. Lett.,* 2012, **68**, 273–276.
6 (a) S. Iijima, M. Yudasaka, R. Yamada, S. Bandow, K. Suenaga, F. Kokai and K. Takahashi, *Chem. Phys. Lett.,* 1999, **309**,165–170; (b) H. Wang, M. Chhowalla, N. Sano, S. Jiaand G.A.J. Amaratunga, *Nanotechnology,* **15**, 2004, 546–550.
7 P. Serp, M. Corrias and P. Kalck, *Appl. Catal.,* 2003, **253**, 337–358.
8 M.C. Bahome, L.L. Jewel, D. Hildebrandt, D. Glasser and N.J. Coville, *Appl. Catal., A,* 2005, **287**, 60–67.
9 Y. Maeda, S. Kimura, M. Kanda, Y. Hirashima, T. Hasegawa, T. Wakahara, Y.F. Lian, T. Nakahodo, T. Tsuchiya and T. Akasaka, J. Lu, X.Zhang, Z. Gao, Y. Yu, S. Nagase, S. Kazaoui, N. Minami, T. Shimizu, H. Tokumoto and R. Saito, *J. Am. Chem. Soc.,* 2005, **127**, 10287–10290.
10 M. Terrones, A. Jorio, M. Endo, A.M. Rao, Y.A. Kim, T. Hayashi, H. Terrones, J.-C. Charlier, G. Dresselhaus and M.S. Dresselhaus, *Mater. Today Magazine,* 2004, **7**, 30–45.
11 Q. Cao and J.A. Rogers, *Adv. Mater.,* 2009, **21**, 29–53.
12 C. Liu, Y.Y. Fan, M. Liu, H.T. Cong, H.M. Cheng and M.S. Dresselhaus, *Science,* 1999, **286**, 1127–1129.
13 H.M. Cheng, Q.H. Yong and C. Liu, *Carbon,* 2001, **39**, 1447–1454.
14 H. Dai, N. Franklin and J. Han, *Appl. Phys. Lett.,* 1998, **73**, 1508–1510.
15 N. Hamada, S. Sawada and A. Oshiyama, *Phys. Rev. Lett.,* 1992, **68**, 1579–1581.
16 R. Saito, M. Fujita, G. Dresselhaus and M.S. Dresselhaus, *Phys. Rev. B,* 1992, **46**, 1804–1811.
17 X. Wang, Y. Liu, G. Yu, C. Xu and J. Zhang, *J. Phys. Chem. B.,* 2001, **105**, 9422–9425.
18 J.Y. Lao, W.Z. Li, J.G. Wen and Z.F. Ren, *Appl. Phys. Lett.,* 2002, **80**, 500–502.
19 J.W. Jang, C.E. Lee, S.C. Lyu, T.J. Lee and C.J. Lee, *Appl. Phys. Lett.,* 2004, **84**, 2877–2879.
20 O. Stephan and P. Ajayan, *Science,* 1994, **266**, 1863–1865.
21 R. Czerw, M. Terrones, J.-C. Charlier, X. Blasé, B. Foley, R. Kamalakaran, N. Grobert, H. Terrones, D. Tekleab, P.M. Ajayan, W. Blau, M. Ruhleand D.L. Carroll, *Nano Lett.,* 2001, **9**, 457–460.
22 M. Terrones, P.M. Ajayan, F. Banhart, X. Blase, D.L. Carroll, J.-C. Charlier, R. Czerw, B. Foley, N. Grobert, R. Kamalakaran, P. Kohler-Redlich, M. Ruhle, T. Seeger and H. Terrones, *Appl. Phys. A Mater.,* 2002, **74**, 355–361.
23 M. Yudasaka, R. Kikuchi, Y. Ohki and S. Yoshimura, *Carbon,* 1997, **35**, 195–201.
24 R. Sen, B.C. Satishkumar, A. Govindaraj, K.R. Harikumar, G. Raina, J.P. Zhang, A.K. Cheetham and C.N.R. Rao, *Chem. Phys. Lett.,* 1998, **287**, 671–676.
25 K. Gong, F. Du, Z. Xia, M. Durstockand L. Dai, *Science,* 2009, **323**, 760–764.
26 E.N. Nxumalo, V.O. Nyamori and N.J. Coville, *J. Organomet. Chem.,* 2008, **693**, 2942–2948.
27 A.L. Elías, J.C. Carrero-Sanchez, H. Terrones, M. Endo, J.P. Lacletteand M. Terrones, *Small,* 2007, **3**, 1723–1729.
28 M. Glerup, J. Steinmetz, D. Samaile, O. Stephan, S. Enouz, A. Loiseau, S. Rothand P. Bernier, *Chem. Phys. Lett.,* 2004, **387**, 193–197.
29 Y. Zhang, H. Gu, K. Suenaga and S. Iijima, *Chem. Phys. Lett.,* 1997, **279**, 264–268.

30 D. Golberg, Y. Bando, W. Han, K. Kurashima and T. Sato, *Chem. Phys. Lett.,* 1999, **308**, 337–342.

31 S.H. Lim, H.I. Elim, X.Y. Gao, A.T.S. Wee, W. Ji, J.Y. Lee and J. Lin, *Phys. Rev. B,* 2006, **73**, 045402/1–045402/6.

32 M. Terrones, N. Grobert, J. Olivares, J.P. Zhang, H. Terrones, K. Kordatos, W.K. Hsu, J.P. Hare, P.D. Townsend, K. Prassides, A.K. Cheetham, H.W. Kroto and D.R.M. Walton, *Nature,* 1997, **388**, 52–55.

33 K. Suenaga, M. Yudasaka, C. Colliex and S. Iijima, *Chem. Phys. Lett.,* 2000, **316**, 365–372.

34 Y. Hao, L. Qingwen, Z. Jinand Liu. Zhongfan, *Chem. Phys. Lett.,* 2003, **380**, 347–351.

35 R. Xue, Z. Sun, L. Su and X. Zhang, *Catal. Lett.,* 2010, **135**, 312–320.

36 K. Chizari, I. Janowska, M. Houllé, I. Florea, O. Ersen, T. Romero, P. Bernhardt, M.J. Ledoux and, C. Pham-Huu, *Appl. Catal., A,* 2010, **380**, 72–80.

37 K.-Y. Chun, H.S. Lee and C.J. Lee, *Carbon,* 2009, **47**, 169–177.

38 W.-X. Lv, K.-Y. Shi, L. Li and S.-Z. Shao, *Microchim. Acta,* 2010, **170**, 91–98.

39 C.J. Lee and J. Park, *Appl. Phys. Lett.,* 2000, **77**, 3397–3399.

40 M.H. Kuang, Z.L. Wang, X.D. Bai, J.D. Guo and E.G. Wang, *Appl. Phys. Lett.,* 2000, **76**, 1255–1257.

41 S.D. Mhlanga, K.C. Mondal, R. Carter, M.J. Witcomb and N.J. Coville, *S. Afr. J. Chem.,* 2009, **62**, 67–76.

42 C.J. Lee. J. Park and J.A. Yu, *Chem. Phys. Lett.,* 2002, **360**, 250–255.

43 C.-T. Hsieh, Y.-T. Lin, J.-Y. Lin and J.-L. Wei, *Mater. Chem. Phys.,* 2009, **114**, 702–708.

44 E. Couteau, K. Hernadi, J.W. Seo, L. Thin-Nga, Cs. Mikó, R. Gaál and L. Forró, *Chem. Phys. Lett.,* 2003, **378**, 9–17.

45 C.H. See, A. Husin and A.T. Harris, *Chem. Eng. Technol.,* 2009, **32**, 1280–1284.

46 J. Cheng, X. Zhang, Z. Luo, F. Liu, Y. Ye, W. Yin, W. Liu and Y. Han, *Mater. Chem. Phys.,* 2006, **95**, 5–11.

47 H. Kathyayini, N. Nagaraju, A. Fonseca and J.B. Nagy, *J. Mol. Catal.,* 2004, **223**, 129–136.

48 E. Dervishi, Z. Li, A.R. Biris, D. Lupu, S.S. Ttrigwell and A.S. Biris, *Chem. Mater.,* 2007, **19**, 179–184.

49 T.C. Schmitt, A.S. Biris, D.W. Miller, A.R. Biris, D. Lupu, S.S. Trigwell and, Z.U. Rahman, *Carbon,* 2006, **44**, 2032–2038.

50 P. Piedigrosso, Z. Konya, J.-F. Colomer, A. Fonseca, G. van Tendeloo and J.B. Nagy, *Phys. Chem. Chem. Phys.,* 2000, **2**, 163–170.

51 D. Pradhan and M. Sharon, *Mater. Sci. Eng. B.*, 2002, **96**, 24–28.

52 A.-C. Dupuis, *Prog. Mater. Sci.,* 2005, **50**, 929–961.

53 R.M. Yadav, P.S. Dobal, T. Shripathi, R.S. Katiyar and O.N. Srivastava, *Nanoscale Res. Lett.,* 2009, **4**, 197–203.

54 P. Ghosh, M. Zamri, M. Subramanian, T. Soga, T. Jimbo, R. Katoh and M. Tanemura, *J. Phys. D: Appl. Phys.,* 2008, **41**, 155405–155412.

55 A.A. Deshmukh, S.D. Mhlanga and N.J. Coville, *Mater. Sci. Eng. R,* 2010, **70**, 1–28.

56 C.J. Lee. S.C. Lyu, H.W. Kim, J.H. Lee and K.I. Cho, *Chem. Phys. Lett.,* 2002, **359**, 115–120.

57 J.-Y. Miao, D.W. Hwang, K.V. Narasimhulu, P.-I. Lin, Y.-T. Chen, S.-H. Lin and L.-P. Hwang, *Carbon,* 2004, **42**, 813–822.

58 (a) A. Romero, A. Garrido, A. Nieto-Márquez, A. Raquel de la Osa, A. de Lucas and J.L. Valverde, *Appl. Catal., A,* 2007, **319**, 246–258; (b) M.M. Shaijumon and S. Ramaprabhu, *Int. J. Hydrogen Energy,* 2005, **30**, 311–317; (c) S. Lim, A. Shimizu, S.-H. Yoon, Y. Korai and I. Mochida, *Carbon,* 2004, **42**, 1279–1283.

59 M. Chen, H.-W. Yu, J.-H. Chen and H.-SKoo, *Diamond Relat. Mater.,* 2007, **16**, 1110–1115.

60 M.A.M. Motchelaho, H. Xiong, M. Moyo, L.L. Jewel and N.J. Coville, *J. Mol. Catal. A:* Chem., 2011, **335**, 189–198.

61 J.H. Lehman, M. Terrones, E. Mansfield, K.E. Hurst and, V. Meunier, *Carbon,* 2011, **49**, 2581–2602.

62 B.J. Landi, C.D. Cress, C.M. Evans and R.P. Raffaelle, *Chem. Mater.,* 2005, **17**, 6819–6834.

63 Z.J. Shi, Y.F. Lian, F.H. Liao, X.H. Zhou, Z.N. Gu, Y. Zhang, S. Iijima, H.D. Li, K.T. Yue and S.L. Zhang, *J. Phys. Chem. Solids,* 2000, **61**, 1031–1036.

64 Q. Liu, W. Ren, F. Li, H. Cong and H.-M. Cheng, *J. Phys. Chem. C,* 2007, **111**, 5006–5013.

65 I.W. Chiang, B.E. Brinson, A.Y. Huang, P.A. Willis, M.J. Bronikowski, J.L. Margrave, R.E. Smalley and R.H. Hauge, *J. Phys. Chem. B,* 2001, **105**, 8297–8301.

66 S.B. McKee and K.S. Vecchio, *J. Phys. Chem. B,* 2006, **110**, 1179–1186.

67 E.N. Nxumalo, P.J. Letsoalo, L.M. Cele and N.J. Coville, *J. Organomet. Chem.,* 2010, **695**, 2596–2602.

68 (a) X. Ma and E.G. Wang, *Appl. Phys. Lett.,* 2001, **78**, 978–980; (b) S. Maldonado, S. Morin and K.J. Stevenson, *Carbon,* 2006, **44**, 1429–1437; (c) S. Choi, K.H. Park, S. Lee and K.H. Koh, *J. Appl. Phys.,* 2002, **92**, 4007–4011.

69 Z. Li, E. Dervishi, Y. Xu, V. Saini, M. Mahmood, O.D. Oshin, A.R. Biris and A.S. Biris, *Catal. Lett.,* 2009, **131**, 356–363.

70 D.K. Singh, P.K. Iyer and P.K. Giri, *J. Appl. Phys.,* 2010, **108**, 084313/1-084313/10.

71 S. Dube and N.J. Coville, *to be published.*

72 G.F. Malgas, C.J. Arendse, N.P. Cele and F.R. Cummins, *J. Mater. Sci.,* 2008, **43**, 1020–1025.

73 S. van Dommele, A. Romero-Izquirdo, R. Brydson, K.P. de Jong and J.H. Bitter, *Carbon,* 2008, **46**, 138–148.

74 H.C. Choi, S.Y. Bae, W.S. Jang, J. Park, H.J. Song, H.-J. Shin, H. Jung and J.-P. Ahn, *J. Phys. Chem. B,* 2005, **109**, 1683–1688.

75 P. Ayala, A. Grüneis, T. Gemming, B. Büchner, M.H. Rümeli, D. Grimm, J. Schumann, R. Kaltofen, F.L. Freire Jr, H. D. Fonseca Filho and T. Pichler, *Chem. Mater.,* 2007, **19**, 6131–6137.

76 J.R. Pels, F. Kapteijn, J.A. Moulijin, Q. Zhu and K.M. Thomas, *Carbon,* 1995, **33**, 1641–1653.

77 A.E. Shalagina, Z.R. Ismagilov, O.Y. Podyacheva, R.I. Kvon and V.A. Ushakov, *Carbon,* 2007, **45**, 1808–1820.

78 M. He, S. Zhou, J. Zhang, Z. Liu and C. Robinson, *J. Phys. Chem. B,* 2005, **109**, 9275–9279.

79 C. Tang, Y. Bando, D. Golberg and F. Xu, *Carbon,* 2004, **42**, 2625–2633.

Supplementary material to:

Z.N. Tetana, S.D. Mhlanga, G. Bepete, R.W.M. Krause and N.J. Coville, *S. Afr. J. Chem.,* 2012, **65**, 39–49.

Carbon yield calculation:

$$\%\mathbf{yield} = \frac{moles\ of\ carbon\ in\ product}{moles\ of\ carbon\ in\ C_2H_2 - \mathbf{moles\ of\ carbon\ in\ CH_3CN}} \times 100\%$$

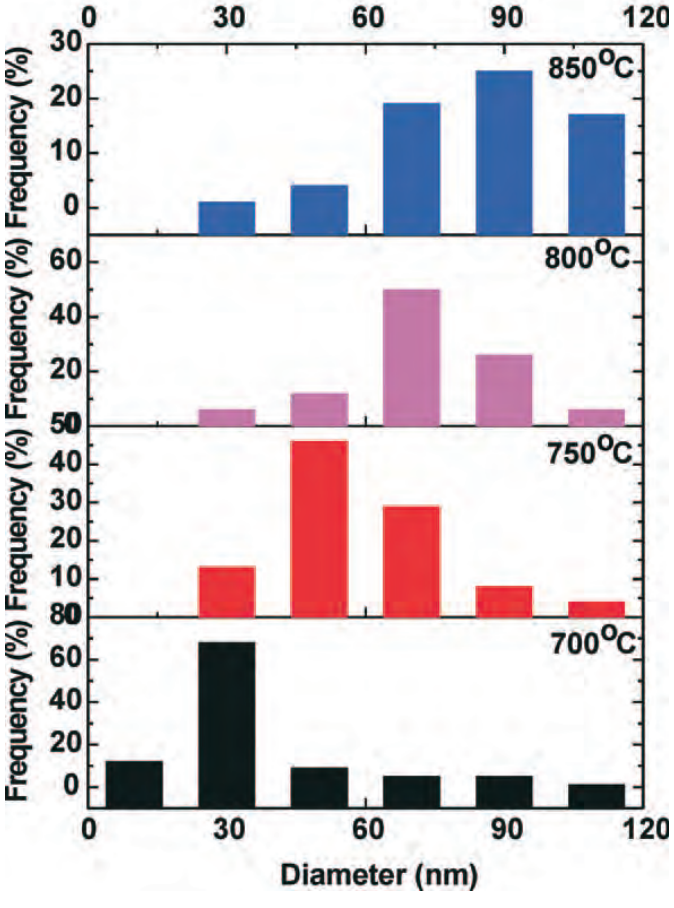

Figure S1a Diameter distributions of the purified N-MWCNTs grown at 700–850 °C using CH_3CN at r.t.

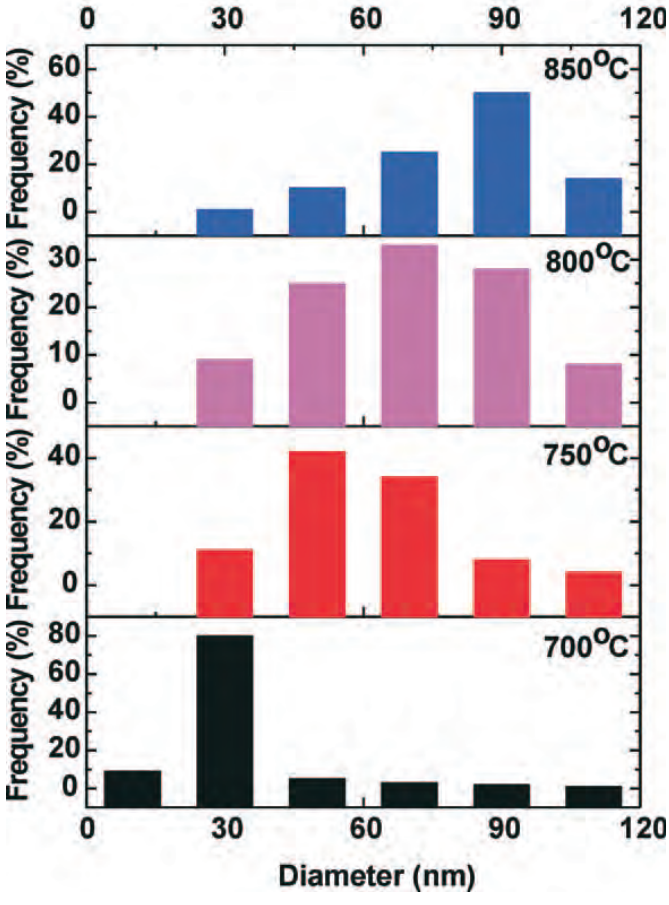

Figure S1b Diameter distributions of the purified N-MWCNTs grown at 700–850 °C using CH_3CN at 50 °C.

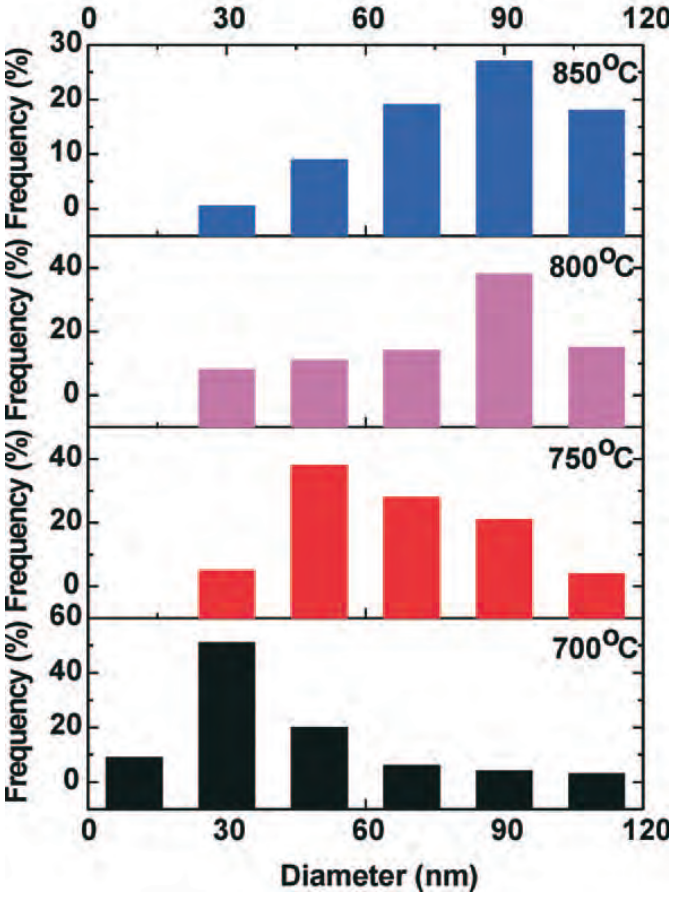

Figure S1c Diameter distributions of the purified N-MWCNTs grown at 700–850 °C using CH_3CN at 80 °C.

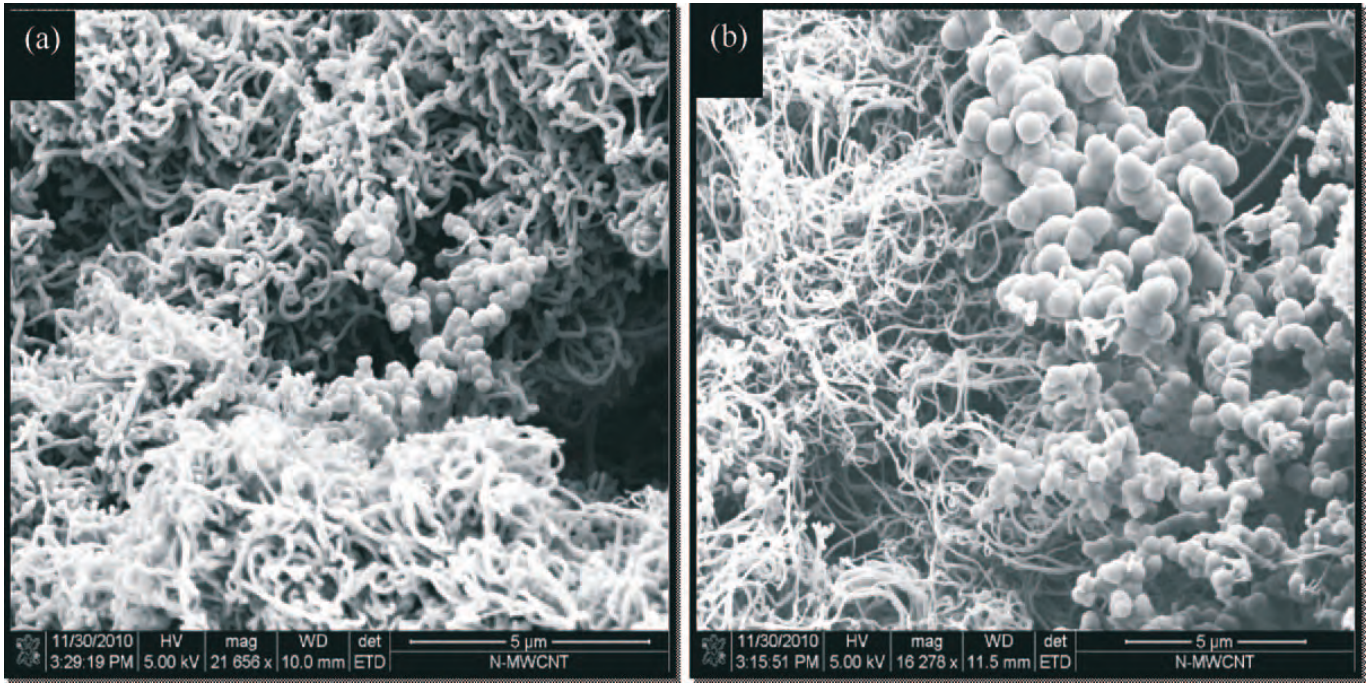

Figure S2 SEM images of the purified N-MWCNTs grown using CH_3CN at 80 °C: (**a**) 800 °C and (**b**) 850 °C.

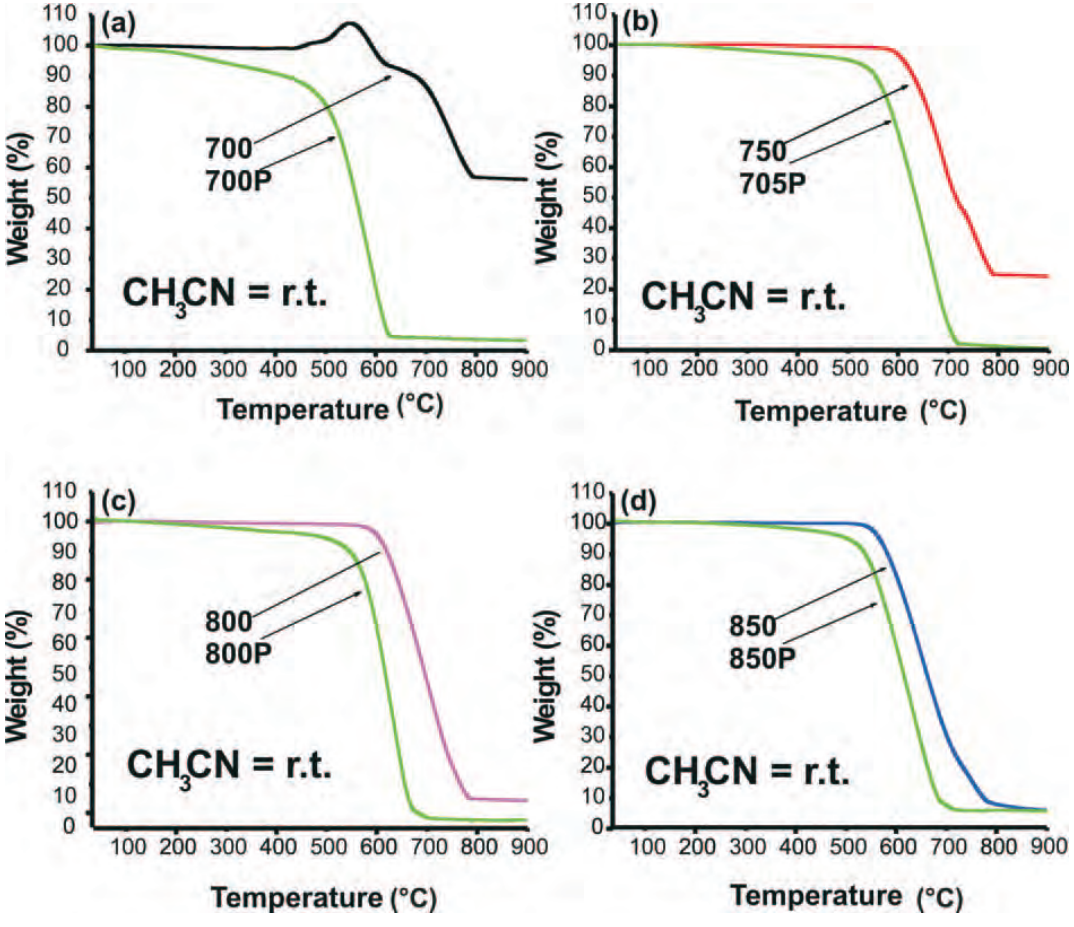

Figure S3 TGA curves of the as-synthesized and purified N-MWCNTs grown at 700–850 °C using CH_3CN at r.t.

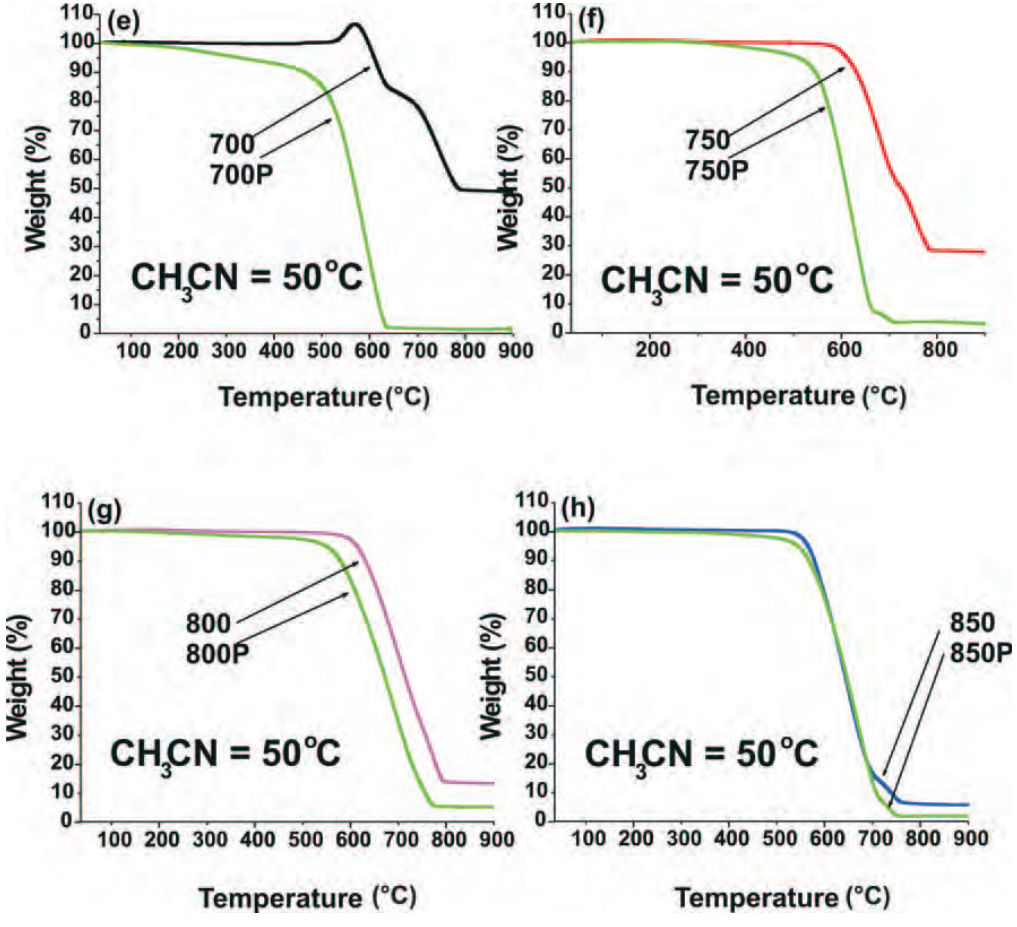

Figure S4 TGA curves of the as-synthesized and purified N-MWCNTs grown at 700–850 °C using CH_3CN at 50 °C.

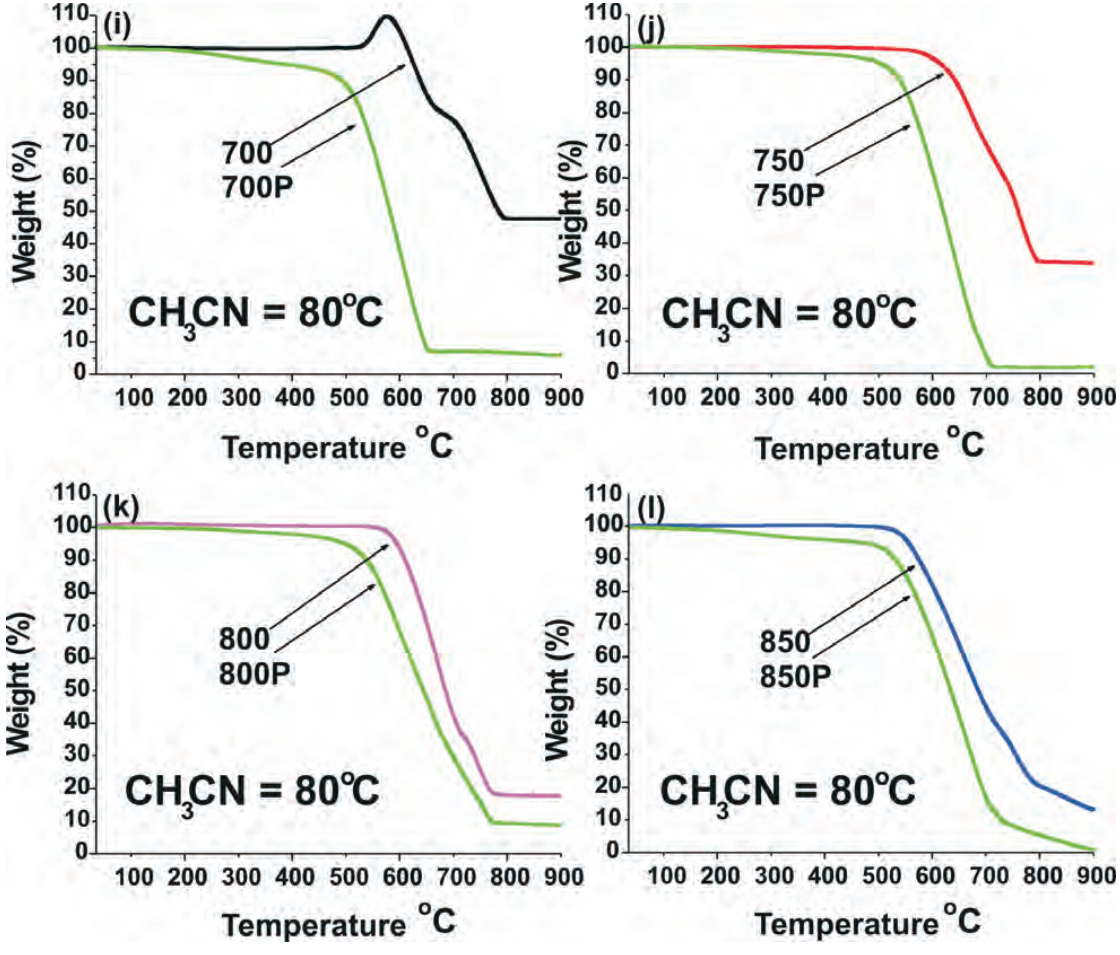

Figure S5 TGA curves of the as-synthesized and purified N-MWCNTs grown at 700–850 °C using CH_3CN at 80 °C.

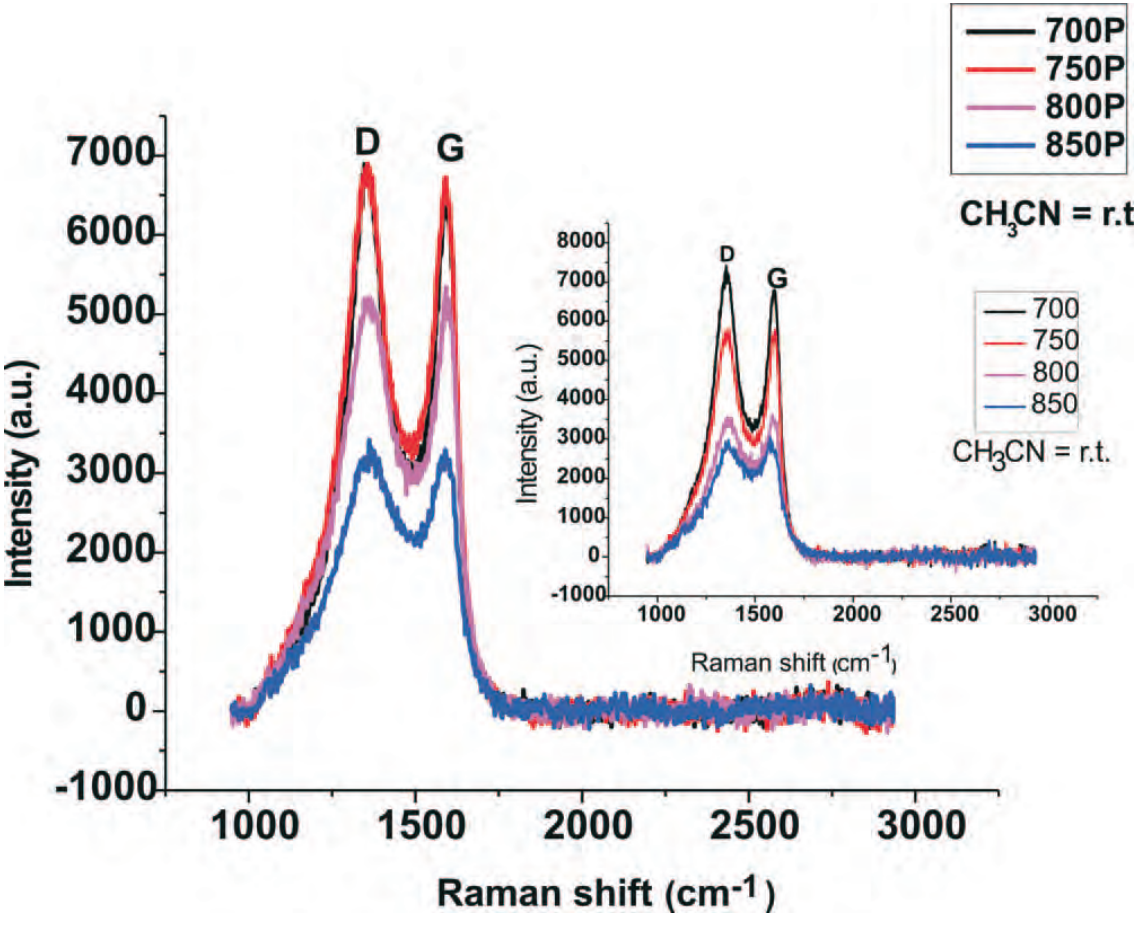

Figure S6 Raman spectra of the purified (700P–850P) and as-synthesized (700–850, inset) N-MWCNTs using CH_3CN at r.t.

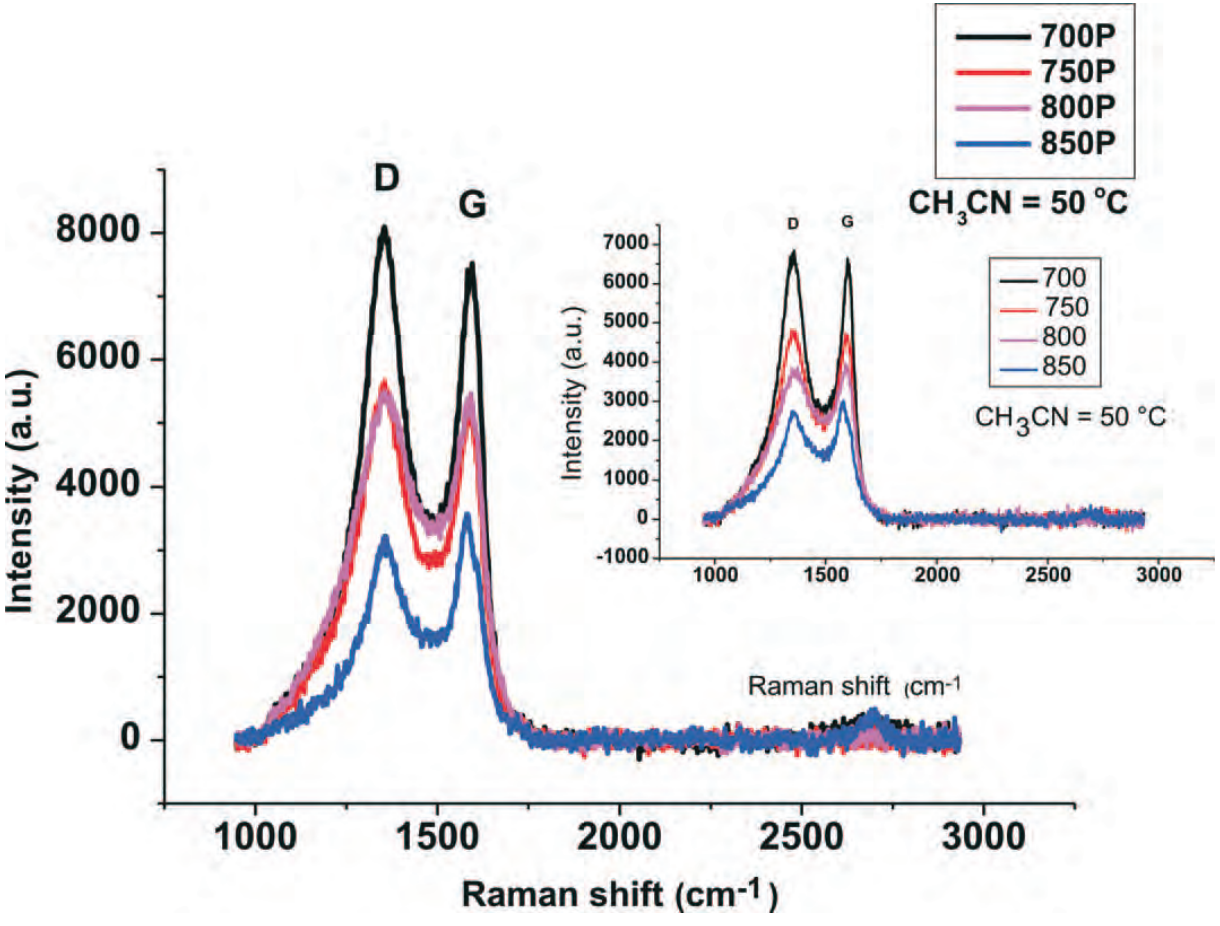

Figure S7 Raman spectra of the purified (700P–850P) and as-synthesized (700–850, inset) N-MWCNTs using CH_3CN at 50 °C.

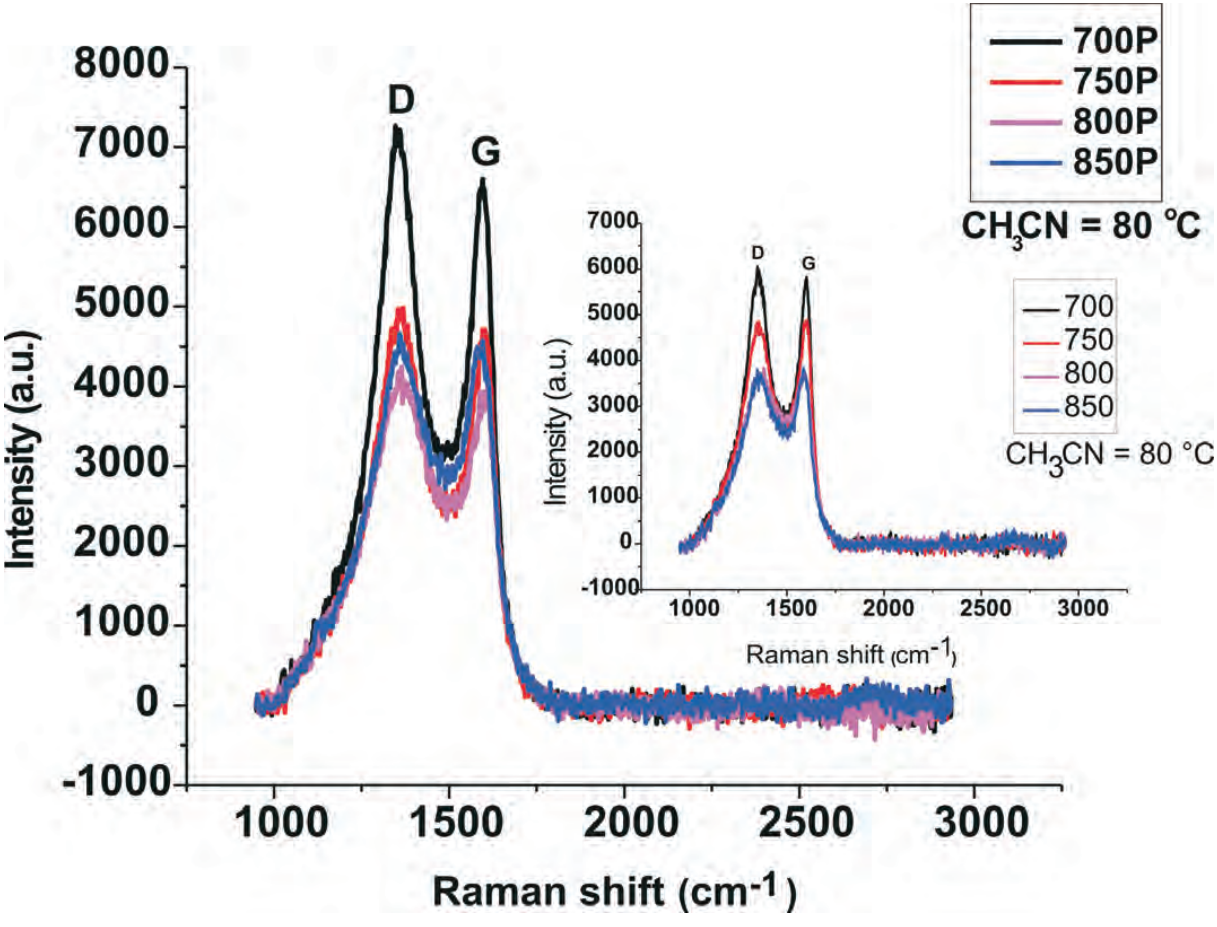

Figure S8 Raman spectra of the purified (700P–850P) and as-synthesized (700–850, inset) N-MWCNTs using CH_3CN at 80 °C.

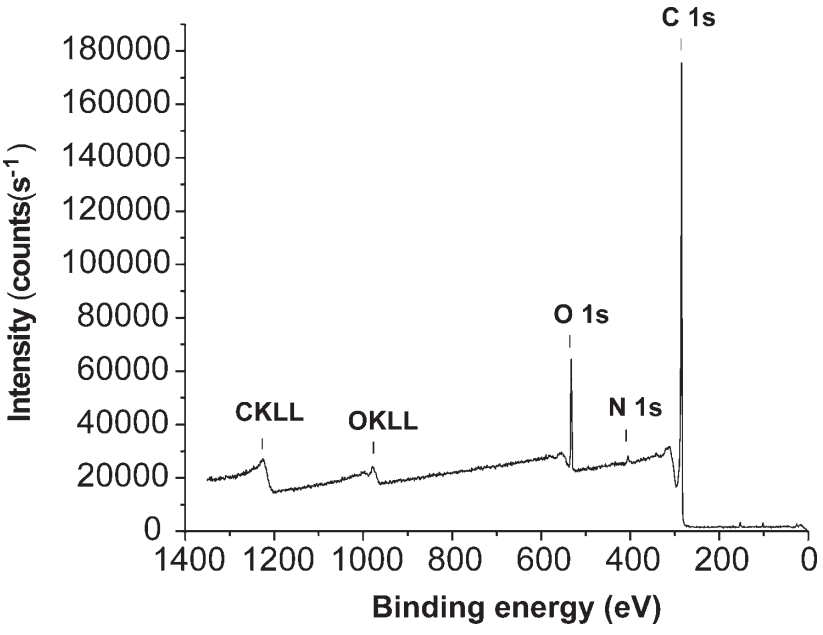

Figure S9 XPS spectra of the purified N-MWCNTs synthesized at 800 °C using CH_3CN at r.t.